Critical behavior of the paramagnetic to antiferromagnetic transition in orthorhombic and hexagonal phases of RMnO$_3$ (R = Sm, Tb, Dy, Ho, Er, Tm, Yb, Lu, Y)

A. Oleaga,[1,*] A. Salazar,[1] D. Prabhakaran,[2] J.-G. Cheng,[3] and J.-S. Zhou[3]

[1]*Departamento de Física Aplicada I, Escuela Técnica Superior de Ingeniería, Universidad del País Vasco UPV/EHU, Alameda Urquijo s/n, 48013 Bilbao, Spain*

[2]*Department of Physics, Clarendon Laboratory, University of Oxford, Oxford OX1 3PU, Uinted Kingdom*

[3]*Materials Science and Engineering Program/Mechanical Engineering, University of Texas at Austin, Austin, Texas 78712, USA*

The critical behavior of the paramagnetic to antiferromagnetic transition in RMnO$_3$ (R = Sm, Tb, Dy, Ho, Er, Tm, Yb, Lu, Y) has been studied with an ac photopyroelectric calorimeter, which gives simultaneously the thermal diffusivity and specific heat as a function of temperature with high resolution around the Néel temperature. RMnO$_3$ (R = Sm, Tb, Dy) has an orthorhombic perovskite structure, whereas the other manganites are hexagonal, thus revealing a strong thermal anisotropy. SmMnO$_3$ with type-A antiferromagnetic ordering exhibits a 3D-XY critical behavior, which could be attributed to the peculiar site anisotropy of Sm^{3+} and the exchange interaction between Mn^{3+} and Sm^{3+} ions. The sinusoidal spin ordering in TbMnO$_3$ and DyMnO$_3$ can be phenomenologically described by the 3D-Heisenberg model. Finally, the hexagonal manganites RMnO$_3$ (R = Ho, Er, Tm, Yb, Lu, Y) are close to the 3D-Heisenberg universality class, ruling out the chiral models predicted by the renormalization group theory.

PACS number(s): 75.40.−s, 64.60.Ht, 65.40.−b, 75.50.Ee

I. INTRODUCTION

Manganites R$_{1-x}$A$_x$MnO$_3$ (R = rare earth, A = alkaline earth) are attracting a renewed interest since the discovery of colossal magnetoresistance at certain compositions (see the work by Tokura[1] and references therein for a major review), magnetoelectric effects,[2–4] as well as due to the rich variety of physical phenomena responsible for their extremely complex phase diagrams. In this work we are focusing our attention on the critical behavior of the magnetic transitions in RMnO$_3$ (R = La, . . . ,Lu, Y) as well as on their thermal properties as a function of temperature.

The crystal structure and magnetic properties of parent compounds RMnO$_3$ undergo major changes as a function of the ionic radius (IR) of the rare-earth R^{3+} ions. In the first place, RMnO$_3$ (R = La, . . . ,Dy) have an orthorhombic perovskite structure. As IR decreases from La down to Dy, the structural distortion manifested by the cooperative octahedral-site rotation increases gradually. Within this group, the antiferromagnetic (AF) ordering changes from the type-A for R = La, . . . ,Sm, to a sinusoidal ordering for R = Gd, Tb, and Dy, where the effect of spin frustration causes sinusoidal AF ordering by means of a strong magnetoelastic coupling.[5] As the IR further decreases from Y, Ho to Lu, RMnO$_3$ crystallize into a hexagonal structure if crystals are grown at ambient pressure.[6] The AF coupling between the spins of the Mn^{3+} ions within an (001) plane is frustrated, which lowers the spin-ordering Néel temperature. In the case of R = Gd, Tb, and Dy, it is worth mentioning that, as the temperature decreases from the incommensurate phase, a lock-in transition takes place to enter a ferroelectric phase,[7] confirming the interplay between electric and magnetic phenomena.

The study of the critical behavior of the paramagnetic to AF transition in RMnO$_3$ is a proper way to unveil the underlying physical mechanism responsible for the particular details of the magnetic transitions. The comparison of the experimental values of the critical exponents with the

theoretical models can contribute to ascertain the type of interaction or predominant mechanism of the transition. For the discussion of the critical behavior in orthorhombic perovskites RMnO$_3$, we summarized in Table I the corresponding critical exponents of relevant theoretical models: mean field model, 3D-Heisenberg model, 3D-Ising model, and XY model. In the Heisenberg case there is a range for the critical parameter, as it varies slightly depending on the source.[8–10] In the case of hexagonal manganites, calculations based on renormalization group theory have added two new possible models: Chiral XY and Chiral Heisenberg. The quasi-two-dimensional nature of the hexagonal crystal structure and the geometrical spin frustration of the triangular lattice would give rise to a peculiar critical behavior. For a triangular lattice antiferromagnet with the 120° structure, the twofold degeneracy of chirality (which corresponds to clockwise and counter clockwise spin arrangements) has been predicted to result in two different universality classes for 3D Heisenberg and XY models,[11] for which experimental verification has been obtained in the case of VBr$_2$ and CsMnBr$_3$, respectively.[12] The subtle difference of the critical exponents between these models (also presented in Table I) and the conventional models requires high-resolution measurements in the vicinity of T_N in order to discriminate them.

Due to the weak antiferromagnetism of these manganites, magnetic measurements are not appropriate to study their critical behavior; instead, thermal measurements are much more useful. Besides, the difference in the values and signs of the critical parameters associated with specific heat are much more distinct from model to model, so it is a better mean to discriminate among the universality classes. In particular, ac photopyroelectric (PPE) calorimetry is a technique especially suitable to study the critical behavior of phase transitions as a small temperature gradient in the sample gives rise to a high signal-to-noise ratio in the detector, so the features of the transition in the near vicinity of the critical temperature can be

TABLE I. Magnetic universality classes relevant to $R\text{MnO}_3$.

Universality Class	α	β	γ	ν	A^+/A^-
Mean-field	0	0.50	1	0.50	
3D-Heisenberg	$-0.115, -0.13$	0.36	1.39	0.71	1.52
3D-Ising	0.11	0.33	1.24	0.63	0.52
3D-XY	-0.014	0.34	1.30	0.66	1.06
Chiral Heisenberg	0.24	0.30	1.17	0.59	0.54
Chiral XY	0.34	0.25	1.13	0.54	0.36

studied in a great detail. The usefulness of this technique has been well demonstrated in the study of the critical behavior of second-order magnetic transitions in different materials, for instance: Cr_2O_3,[13] NiO,[14] KMnF_3,[15] $\text{La}_{1-x}\text{Sr}_x\text{MnO}_3$;[16] see the paper by Zammit *et al.*[17] for an in-depth review of its applications.

There are already some studies on the critical behavior of specific heat in certain $R\text{MnO}_3$ manganites. Oleaga *et al.*[18] established that the class of universality in the case of La, Pr, and Nd is the 3D-Heisenberg class by means of the inverse thermal diffusivity and specific heat measurements. YMnO_3 has been studied by Tachibana *et al.*[19] and Katsufuji *et al.*;[20] Tachibana *et al.* have obtained critical values supporting the Heisenberg model, whereas Katsufuji *et al.* obtained an $\alpha = 0.25$. But in both cases the reduced temperature intervals were too narrow to obtain conclusive results. Katsufuji *et al.*[20] have also considered LuMnO_3, but they obtained two different values for α: one for $T > T_N$ and another one for $T < T_N$, which is inconsistent with the renormalization group theory and indicates that they could not obtain a good fitting to the parametric equation. The work we are presenting in this paper is the first comprehensive study of the critical behavior of the AF transition of $R\text{MnO}_3$ in which we include our previous work[18] on $R = $ La, Pr, and Nd and add Sm, Tb, Dy, Ho, Er, Tm, Yb, Lu, and Y from this work in order to see how the changes in the crystal structure and spin ordering structure are reflected in the universality class.

Last, we also intend to characterize the dynamical thermal properties of this family as a function of temperature (for which there are no thermal diffusivity measurements in literature), complementing those already performed on static thermal properties.[6,21]

II. EXPERIMENTAL TECHNIQUES AND SAMPLES

High-resolution ac PPE calorimetry has been successfully used to extract thermal properties both from solid and liquid materials. In particular, using the standard back-detection configuration,[22,23] simultaneous measurements of thermal diffusivity D and specific heat c_p can be carried out. As performed in the laboratory in Spain for the case of solid materials, in this configuration an acousto-optically modulated He-Ne laser beam of 5 mW illuminates the front surface of the sample under study. Its rear surface is in thermal contact with a 350-μm-thick LiTaO_3 pyroelectric detector with Ni-Cr electrodes on both surfaces by using an extremely thin layer of a highly heat-conductive silicone grease. The PPE signal is processed by a lock-in amplifier operating in the current mode.

Both sample and detector are placed inside a closed-cycle He cryostat specially designed to avoid the transmission of mechanical vibrations to the detector (pyroelectric detectors are also piezoelectric) and with the sample in a He atmosphere, allowing a good thermal contact between sample and detector all along the whole temperature range, which is 12–320 K. Cooling/heating rates can be performed from 100 mK/min for measurements on a wide temperature range down to 10 mK/min for high-resolution runs close to the phase transition.

For opaque and thermally thick samples (i.e., the thickness of the sample is higher than the thermal diffusion length $\mu = \sqrt{D/\pi f}$, where f is the modulation frequency of the laser beam) the natural logarithm ($\ln V$) of the amplitude of the normalized PPE signal (which is obtained by dividing the measured signal by the signal provided by the bare detector) and its phase (Ψ) have a linear dependence on $\sqrt{f}$, with the same slope. From their slope m and from the vertical separation between the two straight lines d, the thermal diffusivity and the thermal effusivity ($e = \sqrt{\rho c_p K} = K/\sqrt{D}$) of the sample can be obtained[24]

$$D = \frac{\pi \ell^2}{m^2}, \tag{1}$$

$$e = e_p \left(\frac{2}{\exp(d)} - 1 \right), \tag{2}$$

where ρ is the density, ℓ is the sample thickness, and e_p is the thermal effusivity of the pyroelectric detector.

Once thermal diffusivity and effusivity have been measured at a certain reference temperature (T_{ref}, D_{ref}, e_{ref}), the temperature is changed while recording the amplitude and phase of the pyroelectric signal at a fixed frequency. The temperature dependence of D and e are given by[24,25]

$$D(T) = \left(\frac{1}{\sqrt{D_{\text{ref}}}} - \frac{\Delta(T)}{\ell\sqrt{\pi f}} \right)^{-2} \tag{3}$$

$$e(T) = e_p(T) \left(\frac{1 + \frac{e_{\text{ref}}}{e_p(T_{\text{ref}})}}{\exp[\Delta''(T)]} - 1 \right), \tag{4}$$

where $\Delta(T) = \Psi(T) - \Psi(T_{\text{ref}})$, $\Delta'(T) = \ln V(T) - \ln V(T_{\text{ref}})$, and $\Delta''(T) = \Delta'(T) - \Delta(T)$. It is worth noticing that, with this technique, thermal diffusivity is measured in the direction perpendicular to the sample surface.

Finally, the temperature dependence of specific heat is calculated from the following relation:

$$c_p(T) = \frac{e(T)}{\rho\sqrt{D(T)}}. \tag{5}$$

TABLE II. Thermal diffusivity at room temperature for RMnO$_3$. The data for $R =$ La, Pr, Nd have been taken from Ref. 18.

	La	Pr	Nd	Sm	Tb	Dy	Ho	Er	Tm	Yb	Lu	Y
D parallel to c (mm^2/s)	1.37	1.35	1.67	1.29	1.28	1.09	1.36	1.42	1.27	1.37	1.97	2.21
D perpendicular to c (mm^2/s)	–	–	–	–	–	–	1.00	1.02	0.92	0.90	1.43	1.39

Single-crystal manganites RMnO$_3$ ($R =$ Sm, Tb, Dy, Ho, Er, Tm, Yb, Lu, Y) were grown by the floating-zone technique and slices of thicknesses of about 0.35–0.45 mm were used for the present study. The samples were prepared so that they have well polished, plane-parallel surfaces. In the case of orthorhombic manganites ($R =$ Sm, Tb, Dy) the faces were cut perpendicular to the c axis. For those with the hexagonal structure ($R =$ Ho, Er, Tm, Yb, Lu, Y), we have prepared two disks for each crystal with the surface normal and parallel to the c axis.

III. EXPERIMENTAL RESULTS AND FITTINGS.

In the first place, thermal diffusivity at room temperature was measured for all samples; the results are presented in Table II together with our previous measurements on orthorhombic manganites ($R =$ La, Pr, Nd).[18] Thermal anisotropy in the hexagonal manganites becomes much more distinct, about 30% lower in the direction perpendicular to the c axis than that parallel to the c axis.

The thermal diffusivity as a function of temperature for all samples is presented in Fig. 1. Figure 1(a) includes all
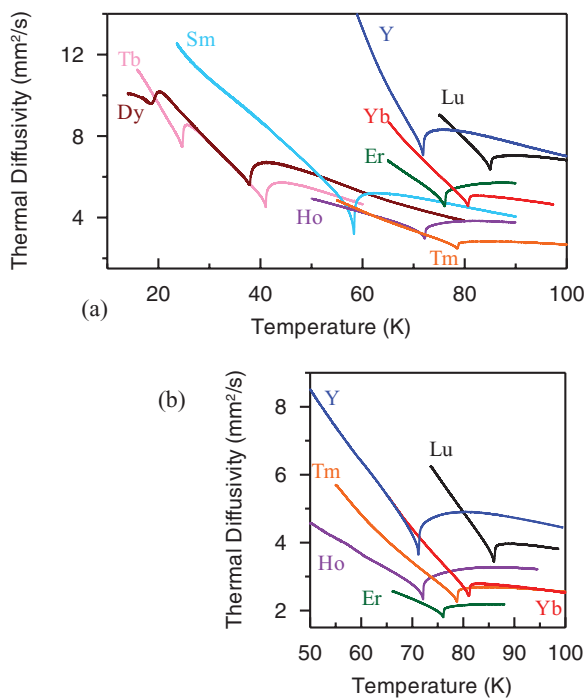

(a)

(b)

FIG. 1. (Color online) (a) Thermal diffusivity as a function of temperature, at low temperatures, for orthorhombic RMnO$_3$ ($R =$ Sm, Tb, Dy) and hexagonal ($R =$ Ho, Er, Tm, Yb, Lu, Y) measured in the c direction. (b) Thermal diffusivity as a function of temperature for hexagonal RMnO$_3$ ($R =$ Ho, Er, Tm, Yb, Lu, Y) measured perpendicularly to the c axis.

of the samples whose faces are perpendicular to the c axis, while Fig. 1(b) shows the hexagonal samples with the face parallel to the c axis. For the hexagonal samples, the features in both directions are similar except for a lower value of thermal diffusivity in the direction perpendicular to the c axis. Again, heat is more effectively transported along the c direction. From a high value at low temperatures, thermal diffusivity quickly decreases as temperature increases. The antiferromagnetic transitions are manifested as obvious dips in the thermal diffusivity curve (59.3 K for Sm, 40.9 K for Tb, 38.1 K for Dy, 72.1 K for Ho, 76.2 K for Er, 78.6 K for Tm, 80.6 K for Yb, 85 K for Lu, and 71.5 K for Y), above which the reduction becomes softer but steady until it reaches the room temperature value shown in Table II, as observed in $R =$ La, Pr, and Nd.[18] The transitions at 24.6 K and 18.6 K observed for Tb and Dy in Fig. 1(a) correspond to the lock-in transition cited in literature.[5] It is worth noting that all the experimental curves are composed of thousands of points, since the measurements were performed at very low rates (down to 10 mK/min); the frequencies at which the measurements have been performed have been chosen so that the thermally thick regime is attained (between 13 and 35 Hz depending on the particular samples).

In order to study the critical behavior in detail, the specific heat curves in the near vicinity of the Néel temperature shown in Fig. 2 have been carefully measured with high resolution. The experimental specific-heat data have been fitted to the well-known relation:

$$c_p = B + Ct + A^{\pm}|t|^{-\alpha}(1 + E^{\pm}|t|^{0.5}), \qquad (6)$$

where $t = (T - T_N)/T_N$ is the reduced temperature, T_N the critical temperature, and α, $A^{\pm}$, B, C, and $E^{\pm}$ are adjustable parameters. Superscripts $+$ and $-$ stand for $T > T_N$ and $T < T_N$, respectively. The linear term represents the background contribution to the specific heat, while the last term is the anomalous contribution to the specific heat. The factor under parenthesis is the correction to scaling that represents a singular contribution to the leading power as known from experiments and theory.[13,26]

The experimental data were simultaneously fitted for $T > T_N$ and $T < T_N$ with a nonlinear least square routine using a Levenberg-Marquardt method. First of all, we selected a fitting range close to the transition while avoiding the rounding part and kept fixed the value of T_N. We performed a first fitting without the correction to scaling term and obtained a set of adjusted parameters. Afterward, we tried to increase the number of data points included in the fitting: first fixing t_{min} and increasing t_{max} and then fixing t_{max} and decreasing t_{min}. The next step was to introduce the correction to scaling term in order to improve the fitting. As a last checking, we let T_N be a free parameter in order to confirm the fitting. In the whole process we focused our attention on the root mean square value as well as on the deviation plot, which is the difference

(a) Orthorhombic Manganites
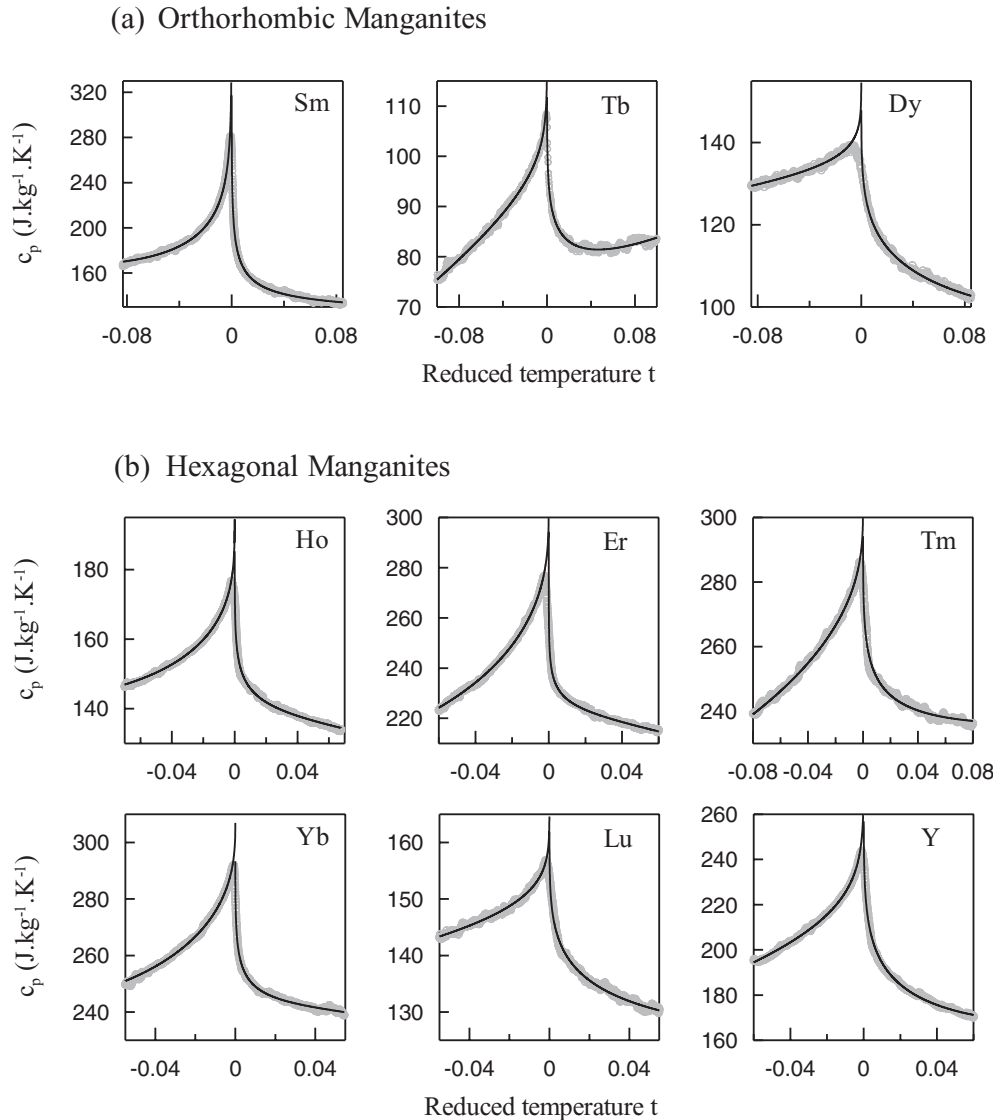

(b) Hexagonal Manganites

FIG. 2. Experimental (dots) and fitted curves (continuous lines) of the specific heat as a function of the reduced temperature for the antiferromagnetic to paramagnetic transition in (a) orthorhombic RMnO$_3$ (R = Sm, Tb, Dy), (b) hexagonal RMnO$_3$ (R = Ho, Er, Tm, Yb, Lu, Y).

between the fitted values and the measured ones as a function of the reduced temperature.

The fitting curves are superimposed to the experimental data points in Fig. 2, in which the dots correspond to the experimental data points (not all of them have been presented, for the sake of clarity) and the continuous lines to the best fitting to Eq. (6). As can be seen in Fig. 2, the fittings are very good. In order to better evaluate the quality of the fittings, Fig. 3 shows for orthorhombic and hexagonal manganites the deviation plots of the fittings with respect to the experimental curves. Again, not all points are presented, for the sake of clarity.

The fitting ranges are in all cases limited by the rounding in the curves; this rounding is inherent to the samples and not attributable to the technique. It is well known that the better the stoichiometric and crystallographic quality of the samples, the smaller the rounding. However, it cannot be completely eliminated (this is why high-quality single crystals are always needed to study critical behavior of phase transitions). With

this particular technique critical behavior studies have been performed in which the fitting range was within 10^{-5} of the reduced temperature,[27] much closer to the critical temperature than in this work, thus indicating that the rounding observed now is inherent to the samples.

The values of the critical parameters, the fitting ranges, and the quality of the fittings given by the root mean square value are presented in Table III.

IV. DISCUSSION

The general evolution of the thermal diffusivity curves and their values are typical for insulating materials in which phonons are mainly responsible for heat transport. From a high value at low temperature, it quickly decreases as temperature is raised because of the reduction in the phonon mean free path. At higher temperatures the reduction is softer until the value attains the one at room temperature. This behavior
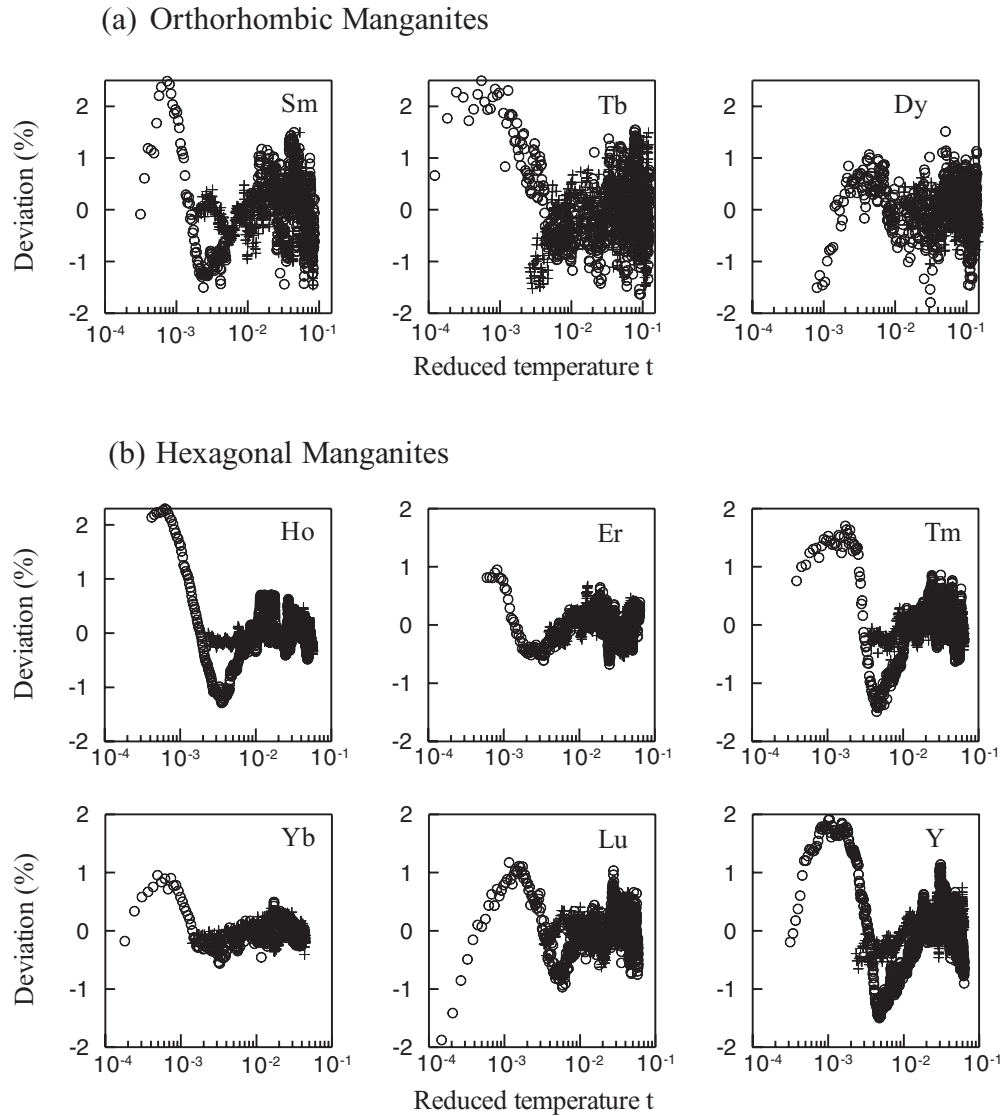
(a) Orthorhombic Manganites

(b) Hexagonal Manganites

FIG. 3. Deviation plots corresponding to the fits in Fig. 2. Open circles are for $T > T_N$ and crosses for $T < T_N$.

in this temperature range agrees well with the one inferred from the thermal conductivity measurements for the hexagonal

manganites by Zhou *et al.*[6] The thermal anisotropy in these RMnO$_3$ samples is also confirmed, which is obviously linked

TABLE III. Critical parameters, fitting ranges, quality of the fittings (given by the root mean square value), and universality class to which the samples are attributed. The data for $R =$ La, Pr, Nd have been taken from Ref. 18.

R ion	α	A^+/A^-	$t_{min} - t_{max}$ $T < T_N$	$t_{min} - t_{max}$ $T > T_N$	R^2	Universality Class
La	-0.11 ± 0.01	1.07				3D-Heisenberg
Pr	-0.11 ± 0.01	1.27				3D-Heisenberg
Nd	-0.11 ± 0.01	1.01				3D-Heisenberg
Sm	-0.013 ± 0.001	1.03	$8.3 \times 10^{-2} - 1.9 \times 10^{-3}$	$2.4 \times 10^{-4} - 8.6 \times 10^{-1}$	0.99804	3D-XY
Tb	-0.09 ± 0.01	1.34	$1.2 \times 10^{-1} - 2.6 \times 10^{-3}$	$1.2 \times 10^{-4} - 1.2 \times 10^{-1}$	0.99267	3D-Heisenberg
Dy	-0.16 ± 0.01	1.71	$1.5 \times 10^{-1} - 1.3 \times 10^{-2}$	$7.9 \times 10^{-4} - 1.4 \times 10^{-1}$	0.99865	Close to 3D-Heisenberg
Ho	-0.14 ± 0.01	2.03	$5.7 \times 10^{-2} - 2.4 \times 10^{-3}$	$4.2 \times 10^{-4} - 5.4 \times 10^{-2}$	0.99763	?
Er	-0.09 ± 0.01	2.29	$5.5 \times 10^{-2} - 3.9 \times 10^{-3}$	$5.9 \times 10^{-4} - 6.3 \times 10^{-2}$	0.99870	?
Tm	-0.19 ± 0.01	2.58	$6.5 \times 10^{-2} - 3.6 \times 10^{-3}$	$3.8 \times 10^{-4} - 6.3 \times 10^{-2}$	0.99313	?
Yb	-0.18 ± 0.01	3.10	$4.5 \times 10^{-2} - 1.6 \times 10^{-3}$	$1.2 \times 10^{-4} - 3.9 \times 10^{-2}$	0.99840	?
Lu	-0.12 ± 0.01	1.41	$5.7 \times 10^{-2} - -3.3 \times 10^{-3}$	$1.2 \times 10^{-4} - 5.9 \times 10^{-2}$	0.99663	3D-Heisenberg
Y	-0.12 ± 0.01	1.37	$6.2 \times 10^{-2} - 2.4 \times 10^{-3}$	$3.1 \times 10^{-4} - 6.3 \times 10^{-2}$	0.99768	3D-Heisenberg

to the crystallographic structure. Heat flow is favored in the c-axis direction.

Concerning the critical behavior presented in Table III, we can divide the $R\mathrm{MnO_3}$ in several subgroups. For $R =$ La, Pr, and Nd, they have a critical parameter α close to the Heisenberg model, but their A^+/A^- ratio is somewhat lower than the theoretical value (1.52). This is no surprise as their magnetic structure (type-A AF ordering) has an intrinsic anisotropy. $\mathrm{SmMnO_3}$ is a very special case because the critical parameters ($\alpha = -0.013$, $A^+/A^- = 1.03$) agrees with the 3D-XY universality class ($\alpha = -0.014$, $A^+/A^- = 1.06$), which corresponds to a two-dimensional behavior. The peak in c_p (and so the dip in the thermal diffusivity) is the strongest one by far in the whole series. This is characteristic of the ion, not of the particular sample, as it was also found by Kimura et al.,[5] though the resolution was not good to extract critical behavior from those data.

The spin arrangement and so the magnetic properties of $\mathrm{SmMnO_3}$ present several features which make it very special among the orthorhombic manganites. In the first place, its ferromagnetism is very weak; its Néel temperature is lowered by 20 K from the previous ion. Among the $R\mathrm{MnO_3}$ samples studied in this work, it is the last one for which the geometrical frustration is not strong enough to change the AF ordering from type-A to some other type. The type-A AF ordering in $\mathrm{LaMnO_3}$ (where there is a small cooperative rotation of the $\mathrm{MnO_6}$ octahedra and a small Jahn-Teller JT splitting $\varepsilon_{\mathrm{JT}}$) is due to the staggered $[d_{3\times^2-r^2}/d_{3y^2-r^2}]$-type orbital order, giving rise to ferromagnetic (FM) (001) planes coupled antiparallel in the c direction. As the IR decreases, the average Mn-O-Mn bond angle decreases and the Mn-O bond lengths are also affected. The spin-spin coupling through $\mathrm{Mn^{3+}}$-O-$\mathrm{Mn^{3+}}$ bonds consists of the t^3-O-t^3 and e^1-O-e^0 superexchange interactions. The weakening of the FM e^1-O-e^0 coupling with decreasing the rare-earth ion radius leads to a competition between the AF t^3-O-t^3 interaction and the FM e^1-O-e^0 interaction in the ab plane, which is responsible for the change in spin ordering. The dominant factor in the weakening of the FM coupling has been shown to be the increase of the JT splitting $\varepsilon_{\mathrm{JT}}$ with decreasing ion radius.[21] The value of the exchange interaction J_{ab} is severely decreased from $\mathrm{LaMnO_3}$ (though still positive, which makes it stay in type-A structure) to $\mathrm{SmMnO_3}$, while J_c keeps more or less constant.

Second, the canted-spin FM moment of the $\mathrm{Mn^{3+}}$-ion array along the c axis produces an exchange field on $\mathrm{Sm^{3+}}$ ion resulting in the $\mathrm{Sm^{3+}}$ magnetic moment aligned antiparallel to the canted-spin direction,[28] unlike other perovskite manganites in which the rare-earth moment is oriented either parallel or orthogonal to the canted-spin direction.[29] As for the overall effect, $\mathrm{SmMnO_3}$ is equivalent to a system whose spin arrangement lies only in the ab plane, which would be better described by the XY universality class, appropriate for planar arrangements.

Depending on the sign of the exchange interaction J_{ab}, the magnetic ordering in the orthorhombic perovskite $R\mathrm{MnO_3}$ is type-A when $J_{\mathrm{ab}} > 0$ and changes to type-E when $J_{\mathrm{ab}} < 0$. (This is the case for the high-pressure orthorhombic phase of $\mathrm{HoMnO_3}$.)[21] At the crossover from positive to negative J_{ab}, the sinusoidal AF spin ordering appears in $\mathrm{TbMnO_3}$ and $\mathrm{DyMnO_3}$, in which an incommensurate low-temperature phase

was observed. Their critical-behavior parameters ($\alpha = -0.09$, $A^+/A^- = 1.34$ and $\alpha = -0.16$, $A^+/A = 1.71$, respectively) are close to the Heisenberg behavior, which means that phenomenologically they behave nearly as isotropic antiferromagnets. Since the spins show no classic ordering, the theoretical development of a universality class, which would take that spin arrangement into account, is needed in order to evaluate the agreement between experiment and theory. To our knowledge, this has not been done yet.

For the $R\mathrm{MnO_3}$ with $r_\mathrm{R} < r_\mathrm{Dy}$, the hexagonal structure is stabilized if the samples are synthesized at ambient pressure. The AF spin coupling within the ab plane is geometrically frustrated because of the triangular lattice structure. As explained in the introduction, the renormalization group theory predicts that $R\mathrm{MnO_3}$ ($R =$ Ho, Er, Tm, Yb, Lu, and Y) should belong to one of the chiral classes.[11] But the obtained experimental parameters clearly rule out that possibility. The obtained α values fall within the range (-0.09, -0.19), while A^+/A^- ratios are between 1.37 and 3.10. The chiral Heisenberg model gives $\alpha = +0.24$ and $A^+/A^- = 0.54$, while the chiral XY gives $\alpha = +0.34$ and $A^+/A = 0.36$. Neither the signs nor the magnitude of the experimental parameters agree with those models. We have tried to perform fittings by fixing the value of the critical parameter α to those of the chiral models in order to evaluate that possibility better. However, it was impossible to obtain proper fittings at all. The six hexagonal $R\mathrm{MnO_3}$ are, nevertheless, subdivided into two subgroups. On the one hand, the critical parameters of Lu ($\alpha = -0.12$, $A^+/A^- = 1.41$) and Y ($\alpha = -0.12$, $A^+/A^- = 1.37$) are very close to those of the Heisenberg universality class, which means that the conventional $\mathrm{Mn^{3+}}$ spin ordering with nonmagnetic rare-earth ions describes well the situation in these samples. This is in agreement with the results on $\mathrm{YMnO_3}$ given by Tachibana et al.,[19] though our fitting range is much closer to the Néel temperature, which validates our critical-behavior analysis. The discrepancy with the chiral models means that the chiral degeneracy must have been removed. Tachibana et al. suggested that the symmetry breaking due to Dzyaloshinskii-Moriya (DM) interactions might be responsible for the loss of chiral degeneracy. DM interactions have also been claimed to be responsible for other magnetic effects in $R\mathrm{MnO_3}$.[30,31] Once the chirality is discarded, as the c axis is quite long (and so these hexagonal crystals have a quasi-two-dimensional structure), the XY model could be the following candidate instead of the Heisenberg class. But there has not been found any magnetic anisotropy in $\mathrm{YMnO_3}$,[32] which supports the isotropic Heisenberg class.

For the case of Ho, Er, Tm, and Yb, although the parameter α is not too far from the Heisenberg class (-0.14, -0.09, -0.19, and -0.18), the ratio A^+/A^- is too high (between 2.03 and 3.10), suggesting that the physical mechanisms responsible for the spin ordering are even more complex. Removal of chirality might happen by means of the DM interactions. Neither an XY model nor the proper Heisenberg model can fully explain the situation, although the data suggests that it is closer to this last one. Unfortunately, there are no magnetic anisotropy measurements performed in these samples, which could help to solve the problem.

The reason why the six hexagonal manganites fall into two subcategories is probably related to the exchange interaction

between the R^{3+} and Mn^{3+} ions. Lu^{3+} and Y^{3+} are nonmagnetic, as they do not have a partially filled $4f$ shell, so this effect is not present. The other four rare-earth ions present magnetic moments along the c axis, perpendicular to the Mn^{3+} spin arrangement. Even though these four manganites present the same magnetic phase of the Mn^{3+} sublattice immediately below the Néel temperature, the detailed phase diagrams and the interaction with the R^{3+} sublattice depend on the particular ion.[33] This exchange interaction might thus modify the symmetry arrangement of the spins, losing the isotropic distribution corresponding to the Heisenberg model and hence the deviations from that model and the differences among all four samples in the particular values of the critical parameters. A thorough experimental work establishing the exact spin arrangement in each case as well as further theoretical development would be needed in order to clarify the exact role played by this mechanism.

V. CONCLUSIONS

RMnO$_3$ manganites (R = Sm, Tb, Dy, Ho, Er, Tm, Yb, Lu, Y) have been studied by means of a high-resolution ac PPE calorimeter. Thermal diffusivity measurements indicate that heat is transferred by phonons and that there is a strong thermal anisotropy in the hexagonal phase of RMnO$_3$, where heat transport is favored in the c direction.

The critical behavior of the paramagnetic to AF transition has been studied by means of detailed specific-heat measurements performed in the near vicinity of the Néel temperature. In the case of SmMnO$_3$ perovskite (which has an AF type-A ordering), the exchange field on the Sm^{3+} site places the rare-earth magnetic moment antiparallel to the canted-spin moment from Mn^{3+} ions, leading to an effectively planar magnetic ordering well described by a 3D-XY critical behavior. The sinusoidal spin ordering in TbMnO$_3$ and DyMnO$_3$ can be phenomenologically described by the Heisenberg model, while both 3D-XY and 3D-Heisenberg chiral universality classes are ruled out in the case of the hexagonal manganites, where the chiral degeneracy could be removed due to the DM interactions. YMnO$_3$ and LuMnO$_3$ belong to the 3D-Heisenberg universality class. The exchange interaction between R^{3+}-Mn^{3+} ions in YbMnO$_3$, TmMnO$_3$, ErMnO$_3$, and HoMnO$_3$ may cause significant deviations from the 3D-Heisenberg universality class

*Corresponding author: alberto.oleaga@ehu.es

[1]Y. Tokura, Rep. Prog. Phys. **69**, 797 (2006).

[2]T. Kimura, T. Goto, H. Shintani, K. Ishizaka, T. Arima, and Y. Tokura, Nature **426**, 55 (2003).

[3]T. Goto, T. Kimura, G. Lawes, A. P. Ramirez, and Y. Tokura, Phys. Rev. Lett. **92**, 257201 (2004).

[4]T. Kimura, G. Lawes, T. Goto, Y. Tokura, and A. P. Ramirez, Phys. Rev. B **71**, 224425 (2005).

[5]T. Kimura, S. Ishihara, H. Shintani, T. Arima, K. T. Takahashi, K. Ishizaka, and Y. Tokura, Phys. Rev. B **68**, 060403(R) (2003).

[6]J.-S. Zhou, J. B. Goodenough, J. M. Gallardo-Amores, E. Morán, M. A. Alario-Franco, and R. Caudillo, Phys. Rev. B **74**, 014422 (2006).

[7]K. Noda, S. Nakamura, J. Nagayama, and H. Kuwahara, J. Appl. Phys. **97**, 10C103 (2005).

[8]J. C. Le Guillou and J. Zinn-Justin, Phys. Rev. B **21**, 3976 (1980).

[9]M. Campostrini, M. Hasenbusch, A. Pelissetto, P. Rossi, and E. Vicari, Phys. Rev. B **63**, 214503 (2001).

[10]M. Campostrini, M. Hasenbusch, A. Pelissetto, P. Rossi, and E. Vicari, Phys. Rev. B **65**, 144520 (2002).

[11]H. Kawamura, J. Phys.: Condens. Matter **10**, 4707 (1998).

[12]M. F. Collins and O. A. Petrenko, Can. J. Phys. **75**, 605 (1997).

[13]M. Marinelli, F. Mercuri, U. Zammit, R. Pizzoferrato, F. Scudieri, and D. Dadarlat, Phys. Rev. B **49**, 9523 (1994).

[14]A. Salazar, M. Massot, A. Oleaga, A. Pawlak, and W. Schranz, Phys. Rev. B **75**, 224428 (2007).

[15]M. Massot, A. Oleaga, A. Salazar, D. Prabhakaran, M. Martin, P. Berthet, and G. Dhalenne, Phys. Rev. B **77**, 134438 (2008).

[16]A. Oleaga, A. Salazar, D. Prabhakaran, and A. T. Boothroyd, Phys. Rev. B **70**, 184402 (2004).

[17]U. Zammit, M. Marinelli, F. Mercuri, S. Paoloni, and F. Scudieri, Rev. Sci. Instrum. **82**, 121101 (2011).

[18]A. Oleaga, A. Salazar, D. Prabhakaran, and A. T. Boothroyd, J. Phys.: Condens. Matter **17**, 6729 (2005).

[19]M. Tachibana, J. Yamazaki, H. Kawaji, and T. Atake, Phys. Rev. B **72**, 064434 (2005).

[20]T. Katsufuji, S. Mori, M. Masaki, Y. Moritomo, N. Yamamoto, and H. Takagi, Phys. Rev. B **64**, 104419 (2001).

[21]J.-S. Zhou and J. B. Goodenough, Phys. Rev. Lett. **96**, 247202 (2006).

[22]M. Marinelli, U. Zammit, F. Mercuri, and R. Pizzoferrato, J. Appl. Phys. **72**, 1096 (1992).

[23]M. Chirtoc, D. Dadarlat, D. Bicanic, J. S. Antoniow, and M. Egée, in *Progress in Photothermal and Photoacoustic Science and Technology*, edited by A. Mandelis and P. Hess (SPIE, Bellingham, Washington, 1997), Vol. 3.

[24]S. Delenclos, M. Chirtoc, A. Hadj Sahraoui, C. Kolinsky, and J. M. Buisine, Rev. Sci. Instrum. **73**, 2773 (2002).

[25]A. Salazar, Rev. Sci. Instrum. **74**, 825 (2003).

[26]A. Kornblit and G. Ahlers, Phys. Rev. B **11**, 2678 (1975).

[27]A. Oleaga, A. Salazar, A. A. Kohutych, and Yu. M. Vysochanskii, J Phys.: Condens. Matter **23**, 025902 (2011).

[28]J.-G. Cheng, J.-S. Zhou, J. B. Goodenough, Y. T. Su, Y. Sui, and Y. Ren, Phys. Rev. B **84**, 104415 (2011).

[29]A. Muñoz, J. A. Alonso, M. J. Martínez López, J. L. García-Muñoz, and M. T. Fernandez-Diaz, J. Phys.: Condens. Matter **12**, 1361 (2000).

[30] E. Hanamura, K. Hagita, and Y. Tanabe, J. Phys.: Condens. Matter **15**, L103 (2003).

[31] A. Muñoz, J. A. Alonso, M. J. Martínez-Lópe, M. T. Casais, J. L. Martínez, and M. T. Fernandez-Diaz, Phys. Rev. B **62**, 9498 (2000).

[32] P. A. Sharma, J. S. Ahn, N. Hur, S. Park, S. B. Kim, S. Lee, J. G. Park, S. Guha, and S.-W. Cheong, Phys. Rev. Lett. **93**, 177202 (2004).

[33] M. Fiebig, Th. Lottermoser, and R. V. Pisarev, J. Appl. Phys. **93**, 8194 (2003).